Doppler Time-of-Flight Rendering Supplementary Material

JUHYEON KIM, Dartmouth College, USA
WOJCIECH JAROSZ, Dartmouth College, USA
IOANNIS GKIOULEKAS, Carnegie Mellon University, USA
ADITHYA PEDIREDLA, Dartmouth College, USA

ACM Reference Format:
Juhyeon Kim, Wojciech Jarosz, Ioannis Gkioulekas, and Adithya Pediredla. 2023. Doppler Time-of-Flight Rendering Supplementary Material. *ACM Trans. Graph.* 42, 6 (December 2023), 7 pages. https://doi.org/10.1145/3618335

1 APPROXIMATION OF ACTUAL PHOTON PATH

We have defined a *geometric path* as a path using scene geometry at time t and used it for the path integral in the main paper. While, we can also define an *actual photon path* as a trajectory followed by a moving photon, which is physically more accurate. However, because an object keeps moving while photons travel, the actual photon path may deviate from the geometric path. Figure 1 illustrates the difference between the geometric path and the actual photon path. Assume that the camera and the directional light source with unit intensity are collocated at $\mathbf{x}_c = \mathbf{x}_e$, and the object is moving away from the camera with constant speed v. Let's say time t as a time when a photon observed at the sensor and $\mathbf{x}(t)$ as the object's position at time t. To determine the elapsed time Δt for the geometric path, we can readily calculate the distance d between the camera and the object as $d_0 + vt$ where $d_0 = \|\mathbf{x}_c - \mathbf{x}(t)\|$ is a constant value. (Fig. 1-(a)). Then,

$$\Delta t = \frac{2d}{c} = \frac{2d_0}{c} + \frac{2v}{c}t, \tag{1}$$

Assuming illumination modulation is $\cos(\omega_g t)$ and ignoring the geometric attenuation, the observed illumination at the sensor at time t is equal to

$$\cos\left(\omega_g\left(t - \Delta t\right)\right) = \cos\left(\omega_g\left(1 - \frac{2v}{c}\right)t - \frac{2d_0}{c}\right). \tag{2}$$

The Doppler frequency shift $\Delta\omega$ could be calculated as

$$\Delta\omega_{\text{geom}} = \frac{2\omega_g v}{c}. \tag{3}$$

Now let's look at the actual photon path (Fig. 1-(b)). We can separately calculate elapsed time from object to camera and light source to object. Let's say each time Δt_1 and Δt_2. Note that because of the principle of constancy of light velocity, the observed photon speed is always c. Then, we can obtain two equations from the photon path from light to object (1)-(3) and object to light (3)-(5)

$$d - v\Delta t_1 = c\Delta t_1, d - v\Delta t_1 = c\Delta t_2. \tag{4}$$

This gives

$$\Delta t_1 = \Delta t_2 = \frac{d}{(c+v)} \tag{5}$$

or,

$$\Delta t_1 + \Delta t_2 = \frac{2d}{(c+v)}. \tag{6}$$

Considering Eq. (2), the actual photon path causes the Doppler frequency shift of

$$\Delta\omega_{\text{actual}} = \frac{2\omega_g v}{(c+v)}. \tag{7}$$

The difference in the Doppler frequency shift between the two paths is $O(v^2/c^2)$, while the Doppler frequency shift itself is $O(v/c)$. Assuming $c \gg v$, we can ignore the deviation due to the discrepancy between the geometric path and the photon's actual path.

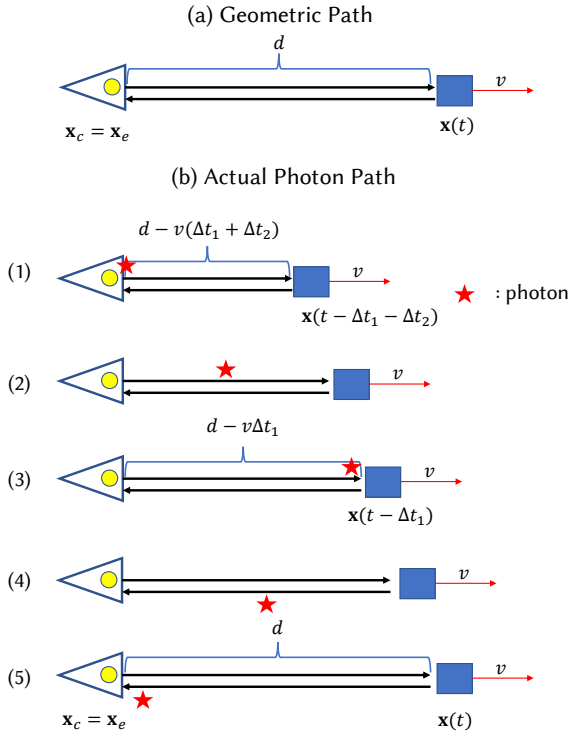

Fig. 1. Geometric path versus actual photon path.

Authors' addresses: Juhyeon Kim, Dartmouth College, USA, juhyeon.kim.gr@dartmouth.edu; Wojciech Jarosz, Dartmouth College, USA, wojciech.k.jarosz@dartmouth.edu; Ioannis Gkioulekas, Carnegie Mellon University, USA, igkioule@cs.cmu.edu; Adithya Pediredla, Dartmouth College, USA, adithya.k.pediredla@dartmouth.edu.

0730-0301/2023/12-ART $15.00
https://doi.org/10.1145/3618335

2 LOW-PASS FILTERING FOR OTHER WAVEFORMS

In the main paper, we ignored the high-frequency term from the multiplication of two sinusoidal sensor and illumination modulation functions, $s(t)$ and $g(t)$. However, for arbitrary periodic signals $s(t)$ and $g(t)$, we can do a similar thing. Let's express each signal using the Fourier series,

$$s(t) = \sum_{n=1}^{\infty} a_n \cos\left(n\omega_s(t+\psi)\right), \tag{8}$$

$$g(t) = g_0 + g_1 \sum_{n=1}^{\infty} b_n \cos\left(n\omega_g t\right). \tag{9}$$

Assuming $\omega_s, \omega_g \gg |\omega_\mathrm{d}|$ where $\omega_\mathrm{d} = \omega_s - \omega_g$, the low-frequency terms of multiplication of modulation functions $s(t)$, $g\left(t - \|\bar{\mathbf{x}}(t)\|\right)$ can be calculated as

$$\frac{g_1}{2} \sum_{n=1}^{\infty} a_n b_n \cos\left(n[\omega_\mathrm{d} t + \psi - \phi(\bar{\mathbf{x}}(t))]\right), \tag{10}$$

where $\phi(\bar{\mathbf{x}}(t)) = -\omega_g \|\bar{\mathbf{x}}(t)\|$. We can calculate the summation of cosine terms as a correlation of two periodic functions,

$$l_s(t') = \sum_{n=1}^{\infty} a_n \cos\left(nt'\right), \quad l_g(t') = \sum_{n=1}^{\infty} b_n \cos\left(nt'\right). \tag{11}$$

where $t' = \omega_\mathrm{d} t + \psi - \phi(\bar{\mathbf{x}}(t))$. l_s and l_g could be also thought of as original modulation signals with the same frequency, ω_d. For some special signals, we can analytically calculate them.

- Sinusoidal : $0.5\cos t'$
- Rectangular : $1 - 2\left(\frac{t'}{\pi}\right)$ for $0 < t' < \pi$
- Triangular : $\frac{1}{3} - 2\left(\frac{t'}{\pi}\right)^2 + \frac{4}{3}\left(\frac{t'}{\pi}\right)^3$ for $0 < t' < \pi$

For rectangular and triangular waves, we only denoted the first half of the signal for convenience. The signal is symmetric at π. If one modulation is a delta function, then the low-pass filtered signal is equal to the other non-delta function. We plot some examples of low-pass filtered signals in Fig. 2.

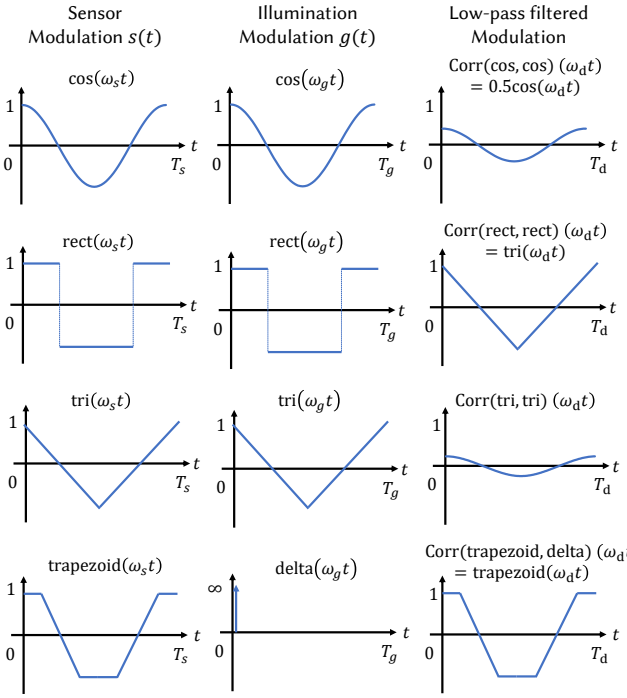

Fig. 2. Low-pass filtered modulation for some signals. Trapezoidal signal is called Hamiltonian in Gupta et al. [2018].

3 DETAILS FOR ANTITHETIC SAMPLING

In this section, we discuss antithetic sampling in detail with mathematical proof. We will mainly focus on shifted antithetic sampling.

3.1 Proof for an Optimal Shift for Shifted Antithetic Sampling

In the main paper, we exploit the fact that shifted antithetic sampling has an optimal value at $t_s = 0.5T$ regardless of frequency or phase offset. We will prove it mathematically in this subsection.

We have defined the variance $\mathrm{Var}(t_s)$ of the antithetic estimator with shift t_s for integration of arbitrary signal $x(t)$ over $[0, T]$ as

$$\mathrm{Var}(t_s) = \int_0^T \left(\frac{x(t) + x\left(\mathrm{mod}(t+t_s, T)\right)}{2} - \mu_x\right)^2 \mathrm{d}t \tag{12}$$

where μ_x is mean of $x(t)$ in $[0, T]$, or ground truth value for the integration. Extracting t_s dependent terms, we are effectively minimizing the following term

$$R(t_s) = \int_0^T x(t)x\left(\mathrm{mod}(t+t_s, T)\right)\mathrm{d}t, \tag{13}$$

which is known as *auto-correlation*. Replacing the modular representation, we can rewrite it as the following equation,

$$R(t_s) = \int_0^{t_s} x(t)x(t - t_s + T)\mathrm{d}t + \int_{t_s}^{T} x(t)x(t - t_s)\mathrm{d}t. \tag{14}$$

One important property of $R(t_s)$ is that it is symmetric over $t_s = 0.5T$. To prove this, define the first term of $R(t_s)$ as $F(t_s)$,

$$F(t_s) = \int_0^{t_s} x(t)x(t - t_s + T)\mathrm{d}t. \tag{15}$$

Then, we can find that the second term is equal to $F(T - t_s)$

$$\begin{aligned} F(T - t_s) &= \int_0^{T - t_s} x(t)x(t + t_s)\mathrm{d}t \\ &= \int_{t_s}^{T} x(t' - t_s)x(t')\mathrm{d}t' \\ &\text{where } t' = t + t_s. \end{aligned} \tag{16}$$

Therefore, $R(t_s) = F(t_s) + F(T - t_s)$ and this infers $R(t_s) = R(T - t_s)$. Another interesting property is that R has a global maximum at $t_s = 0$ regardless of $x(t)$. This could be shown using *rearrangement inequality*.

Our goal is to find an optimal t_s that minimizes $R(t_s)$. Generally, finding such globally optimal t_s is not straightforward, but we can find it for some special functions, and the sinusoidal function is one of them. Let's express $R(t_s)$ using $x(t) = \cos(\omega t + \phi)$. In the main manuscript, it was $x(t) = \cos(\omega_\mathrm{d} t + \theta)$, but we will use

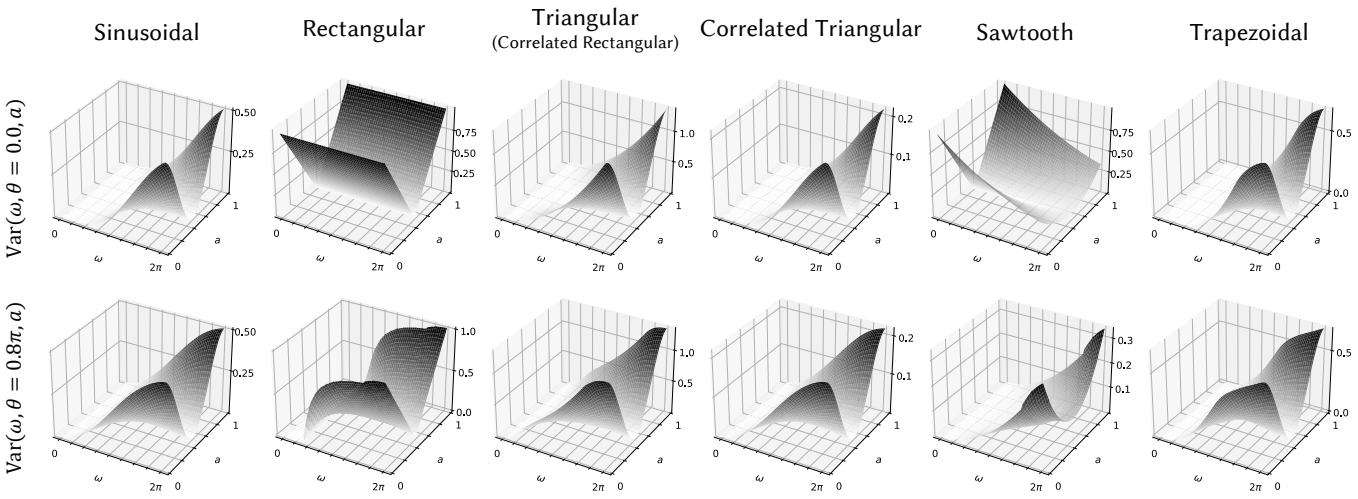

Fig. 3. Variance of using different antithetic shift a for different ω, θ. We plotted for a total of 6 different waveforms at $\theta = 0, 0.8\pi$.

$x(t) = \cos(\omega t + \phi)$ instead for convenience. Also, for simplicity, let's assume $T = 1$ without loss of generality and denote $t_s = a$.

Then,

$$R(a) = \int_0^a \cos(\omega t + \phi)\cos(\omega(t + 1 - a) + \phi)\mathrm{d}t + \int_a^1 \cos(\omega t + \phi)\cos(\omega(t - a) + \phi)\mathrm{d}t \tag{17}$$

and

$$F(a) = \int_0^a \cos(\omega t + \phi)\cos(\omega(t + 1 - a) + \phi)\mathrm{d}t. \tag{18}$$

Because

$$\begin{aligned} &2\int_x^y \cos(\omega(t - c) + \phi)\cos(\omega(t - d) + \phi)\mathrm{d}t \\ &= (\cos(\omega(y + x) + 2\phi - \omega(c + d))\sin(\omega(y - x))) \\ &+ (y - x)\cos(\omega(c - d)), \end{aligned} \tag{19}$$

we can rewrite $F(a)$ as following:

$$F(a) = \frac{1}{2\omega}\cos(\omega + 2\phi)\sin(\omega a) + \frac{a}{2}\cos(\omega(1 - a)). \tag{20}$$

Our intuition is that $R(a)$ has a minimum value at $a = 0.5$. Because $R(a)$ is symmetric at $a = 0.5$, we can show that $R(a)$ has a minimum at $a = 0.5$ if $R'(a) < 0$ for $0 < a < \frac{1}{2}$. Here is our objective:

$$\text{Show that } R'(a) < 0$$
$$\text{Given } 0 < a < \frac{1}{2} \text{ and } 0 < \omega < 2\pi$$

To calculate $R'(a)$, let's first calculate $F'(a)$ and $F'(1 - a)$.

$$F'(a) = \frac{1}{2}\cos(\omega + 2\phi)\cos(\omega a) + \frac{1}{2}\cos(\omega(1 - a)) + \frac{a}{2}\omega\sin(\omega(1 - a)) \tag{21}$$

$$F'(1 - a) = \frac{1}{2}\cos(\omega + 2\phi)\cos(\omega(1 - a)) + \frac{1}{2}\cos(\omega a) + \frac{(1 - a)}{2}\omega\sin(\omega(1 - a)) \tag{22}$$

Because $R(a) = F(a) + F(1 - a)$,

$$\begin{aligned} R'(a) &= F'(a) - F'(1 - a) \\ &= (1 - \cos(2\theta))\sin\left(\frac{\omega}{2}\right)\sin\left(\omega a - \frac{\omega}{2}\right) \\ &+ \frac{1}{2}(\omega\sin(\omega(1 - a)) - (1 - a)\omega\sin(\omega a)) \end{aligned} \tag{23}$$

where $\theta = \phi + 0.5\omega$. Note that such substitution is equivalent with *phase compensation* used in Hu et al. [2022]. We will use θ instead of ϕ from now. Let's examine the first term and the second term separately. We can easily show that the first term is < 0 because,

$$1 - \cos(2\theta) > 0$$
$$\sin\left(\frac{\omega}{2}\right) > 0 \ (\because 0 < \omega < 2\pi)$$
$$\sin\left(\omega a - \frac{\omega}{2}\right) < 0 \left(\because 0 < \omega < 2\pi, 0 < a < \frac{1}{2}\right)$$

The second term is related to sinc function. Let's consider two possible cases.

Case 1. $0 < \omega a < \omega(1 - a) < \pi$. In this case, the sinc function is positive and also a decreasing function.

$$\frac{\sin(\omega a)}{\omega a} > \frac{\sin(\omega(1 - a))}{\omega(1 - a)}$$
$$\therefore a\omega\sin(\omega(1 - a)) - (1 - a)\omega\sin(\omega a) < 0$$

Case 2. $0 < \omega a < \pi < \omega(1 - a) < 2\pi$. In this case, the sign of the two sinc functions are different.

$$\frac{\sin(\omega a)}{\omega a} > 0 > \frac{\sin(\omega(1 - a))}{\omega(1 - a)}$$
$$\therefore a\omega\sin(\omega(1 - a)) - (1 - a)\omega\sin(\omega a) < 0$$

Therefore, we can conclude that

$$R'(a) < 0 \quad \text{for } 0 < a < \frac{1}{2}, 0 < \omega < 2\pi$$

Since $R(a)$ is symmetric at 0.5, showing $R'(a) < 0$ for $0 < a < 0.5$ proves that $R(a)$ has a global minimum at $a = 0.5$.

We plot $\mathrm{Var}(\omega, \theta, a)$ of various functions on Fig. 3. Because R, Var also depends on ω, θ, we added them as a variable. Their shapes vary, but you can easily notice that they are all symmetric over $a = 0.5$ and have a global minimum at $a = 0.5$. Also, we could find that a similar optimal property holds for other waveforms. Although we only show mathematical proof for sinusoidal waves, other waveforms in Fig. 3 could be also mathematically proved that $a = 0.5$ is optimal regardless of ω, θ. However, we will omit the detailed proof because it is just a tedious calculation over several cases considering discontinuities. We could not find the exact condition for $x(t)$ that $a = 0.5$ becomes optimal, but this could be further studied in future work.

3.2 Variance Gain Analysis

We want to know how much variance reduction using the optimal antithetic shift is efficient compared to not using the antithetic sampling. We can rewrite the antithetic estimator's variance for sinusoidal wave as follows,

$$\mathrm{Var}(\omega, \theta, a) = \frac{1}{2}\mu_2^2(\omega, \theta) - \mu^2(\omega, \theta) + \frac{1}{2}R(\omega, \theta, a) \tag{24}$$

where μ and μ_2 are mean and quadratic mean respectively.

To evaluate the worst case variance, we can plot $\mathrm{Var}(\omega, \theta, \frac{1}{2})$ over $\omega \in [0, 2\pi], \theta \in [0, 2\pi]$ and find maximum value. However as variance innately depends on ω, θ, it does not tell the relative effectiveness of using the antithetic sampling. Instead, we can calculate the variance ratio (or gain) compared to the uniform sampling counterpart. The uniform sampling counterpart could be thought of as antithetic sampling with $a = 0$ with double the number of samples, which halves the variance[1]. Therefore, the variance ratio could be calculated as

$$\frac{\mathrm{Var}(\omega, \theta, \frac{1}{2})}{\frac{1}{2}\mathrm{Var}(\omega, \theta, 0)}. \tag{25}$$

The antithetic sampling becomes more effective as the above ratio becomes smaller (equal to gain becomes infinite). The variance and the variance ratio are plotted in Fig. 4. We could notice that using the antithetic sampling is useful for every ω, θ, making the variance less than half compared to uniform sampling. We could also observe the worst case at $\omega = 0$ where the ratio is 0.5 and the best case at $\omega = 2\pi$ where the ratio is 0. This is consistent with our expectation that shifted antithetic sampling is useful for full heterodyne mode while not that useful for homodyne mode. One may wonder why shifted antithetic sampling is not useful for homodyne mode in the rendering case, because it still gives half of the variance compared to uniform sampling. This is because, for lower ω, the path space variance dominates the total variance, and effect of the time-sampling method becomes less noticeable.

[1]We can also calculate this with an MC estimator with two independent uniform samples.

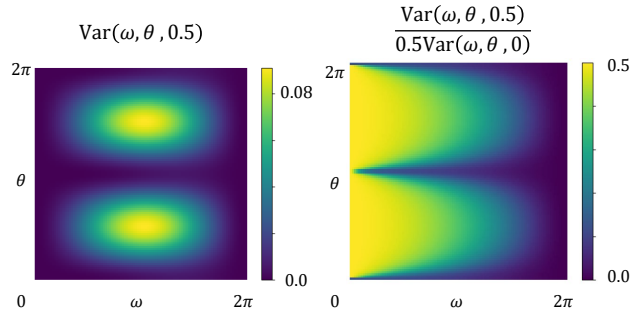

Fig. 4. (Left) Variance of using using $a = 0.5$. (Right) Relative variance compared to uniform sampling counterpart.

3.3 Sinusoidal Wave with Truncate or Geometric Attenuation

The actual signal can be truncated because of discontinuity and also slightly deformed because of geometric attenuation. This could be modeled as follows.

$$x(t) = \begin{cases} \cos(\omega t + \phi_1) \cdot \frac{1}{(l_1 + v_1 t)^2} & \text{if } t < t_d \\ \cos(\omega t + \phi_2) \cdot \frac{1}{(l_2 + v_2 t)^2} & \text{if } t > t_d \end{cases} \tag{26}$$

Note that using the discontinuity option makes the $R(a)$ not optimal at $a = 0.5$ for some ω, ϕ. But instead, at least we can empirically expect that using antithetic sampling with $a = 0.5$ gives the best result on average. We calculated an expected variance using above signal with $l_1, l_2 \in [1, 3], v_1, v_2 \in [-0.01, 0.01], \phi_1, \phi_2 \in [0, 2\pi], t_d \in [0, 1]$. Note that the v value is relatively small because the exposure time is a few ms and object speed is a few m/s, so it has a small value if T is normalized to 1. If the object speed is 5 m/s and exposure time is 2ms, v becomes 0.01. We plotted two results in Fig. 5. The left image shows a configuration that the variance can be a local maximum at $a = 0.5$. The right image shows the averaged variance which has a minimum value at $a = 0.5$, assuming each variable has a uniform distribution. Such observation supports that using $a = 0.5$ is still optimal on average under several possible variations.

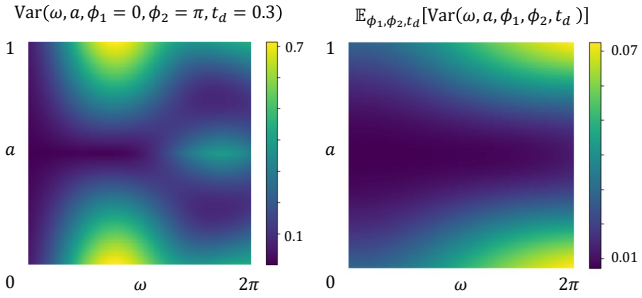

Fig. 5. (Left) Variance under specific configuration that $a = 0.5$ is no longer optimal. (Right) Expectation over all of the variables except a, ω.

3.4 Antithetic Sampling with Higher Frequency

Here, we assumed that $0 < \omega < 2\pi$, but what happens if frequency becomes higher? Variance has a local optimum at $a = 0.5$, but it is not guaranteed to be a global minimum or a local minimum for higher frequency. Our observation is plotted in Fig. 6.

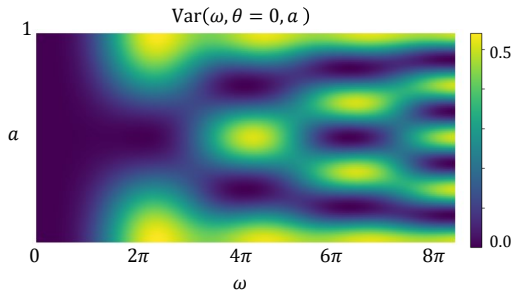

Fig. 6. Variance for higher frequency. For certain ranges, $a = 0.5$ is not a global minimum, but a local maximum.

3.5 Multiple Antithetic Sampling

In the previous subsections, we have demonstrated that antithetic sampling with time shift 0.5 gives an optimal result for sinusoidal wave and also optimal in average with some variations. The question then naturally arises: What if multiple antithetic samples are available?

Interestingly, if we can use N samples, then using antithetic samples with shift $\left[0, \frac{1}{N}, \frac{2}{N}, ..., \frac{N-1}{N}\right]$ seems to minimize the variance of the estimator. Such sampling is also known as *periodic sampling*, *systematic sampling* or *uniform jitter sampling* [Ramamoorthi et al. 2012]. We plot the example of using two antithetic samples with the shift of a, b on Fig. 7. For each case, the global minimum could be observed at $[0.33, 0.66]$. We also could observe that an equal interval shift gives the best result for larger N among several variations without rigorous mathematical proof. Instead, a weaker suggestion, we could show that such periodic sampling has a global minimum if R is convex with regard to a, which could be proved using *Jensen's inequality*.

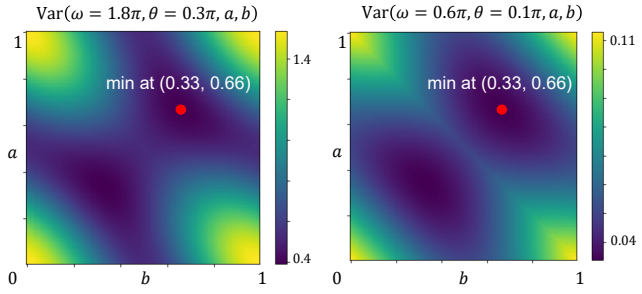

Fig. 7. Variance when using two antithetic samples of a, b. We only show two cases, but it seems that $[0.33, 0.66]$ is also optimal for other cases.

Variance Reduction using Periodic Sampling. Now saying that multiple antithetic sampling is optimal with periodic shift, we want to investigate the effect of variance reduction by using more samples. We plotted the result of the expectation of the variance over both ω, θ in Fig. 8 assuming they both have a uniform distribution. The x-axis means the number of antithetic samples N. We could observe that periodic sampling decreases variance by the rate of $1/N^2$. We also plot other sampling methods, uniform sampling, and stratified sampling in the same figure. For uniform sampling, N means the number of independent samples, and for stratified sampling, N means the number of strata. Uniform sampling decreases variance by the rate of $1/N$ while we found that stratified sampling decreases variance by the rate of $1/N^3$. Such fast variance reduction of stratified sampling makes stratified sampling better than periodic sampling over a certain N. This is not a surprising result because there are no clear antithetic samples that make zero variance for arbitrary frequencies.

However, as pointed out in the main manuscript, increasing the number of correlated time samples reduces diversity in the path domain which eventually increases the total variance. Therefore even though stratified sampling works better than periodic sampling for large N, it does not cause practical advantage in rendering. While, the fact that periodic sampling outperforms others at $N = 2$ (in this case, periodic sampling is the same as shifted antithetic sampling) is more important.

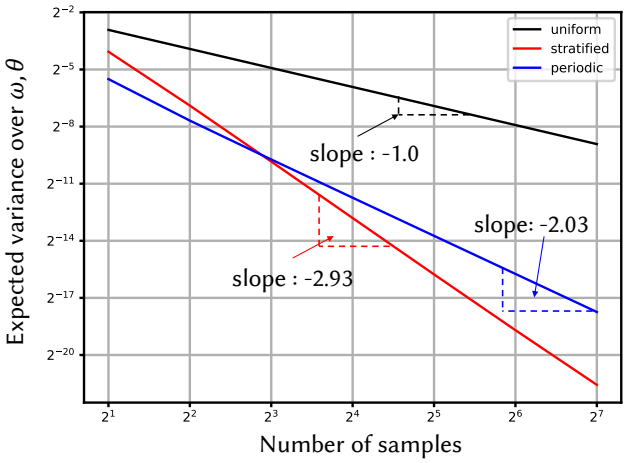

Fig. 8. Variance reduction using more samples for uniform, stratified, and periodic sampling.

3.6 Optimal Antithetic Shift for Other Sampling Methods

The mirrored antithetic sampling mentioned in the main paper does not have a globally optimal antithetic shift regardless of ω, θ. A similar thing happens for stratified sampling, that there is no globally optimal starting point of strata. Usually, a starting point of strata is 0, but to be fair with the shifted antithetic sampling method, we consider a non-zero starting point for stratified sampling. The first row of Fig. 9 shows such non-global optimal property for both sampling methods at $\omega = 2\pi$. Thus, instead, we have considered

the expected variance over uniform θ, $\mathbb{E}_\theta[\mathrm{Var}(\omega, \theta, a)]$, which is shown in the second row of Fig. 9. It shows that mirrored antithetic sampling has an optimal value at $a = 0, 1$, and stratified sampling has an optimal value at $a = 0, 0.5, 1$. Therefore, the optimal shift value of $a = 0$ is used for both mirrored antithetic and stratified sampling.

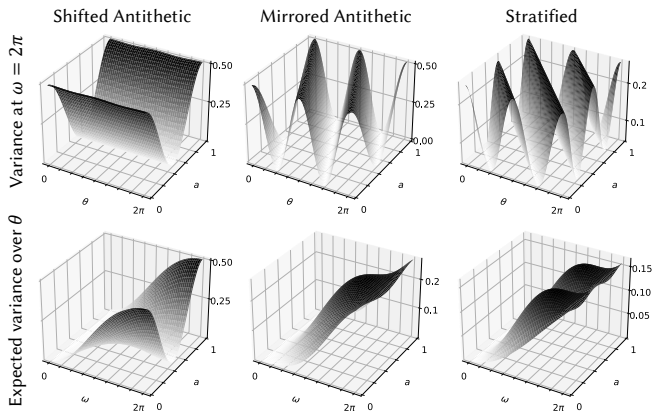

Fig. 9. The effect of shift a for other sampling methods. Note that for mirrored antithetic sampling and stratified sampling, a does not have θ independent optimal value.

Using this optimal shift, we can calculate $\mathbb{E}_\theta[\mathrm{Var}(\omega, \theta)]$ for each sampling method.

- Uniform : $\frac{\pi(\omega^2+2\cos(\omega)-2)}{\omega^2}$
- Stratified : $\frac{\pi(\omega^2+8\cos\left(\frac{\omega}{2}\right)-8)}{2\omega^2}$
- Shifted antithetic : $\frac{\pi(\omega^2+4\cos(\omega)-4)}{2\omega^2} + \frac{\pi}{2}\cos\left(\frac{\omega}{2}\right)$
- Mirrored antithetic : $\frac{\pi(\omega^2+4\cos(\omega)-4)}{2\omega^2} + \frac{\pi}{2}\frac{\sin(\omega)}{\omega}$

Such mathematical expression clearly demonstrates superiority of shifted antithetic in $\omega \in [\pi, 2\pi]$ and mirrored antithetic in $\omega \in [0, \pi]$. Note that this is also plotted in the main paper, Fig.7-(b).

4 ANTITHETIC SAMPLING WITH MIS

In this section, we will discuss antithetic sampling with MIS (multiple importance sampling). Although antithetic sampling is not exactly an importance sampling, let us just call it as MIS for convenience. Let's think about the following integration,

$$I = \int_X f(x)\mathrm{d}x. \tag{27}$$

Without loss of generality, we can say that $I = 0$ for simplicity. If not, we can add a constant value to $f(x)$. Let's also define the bijective antithetic mapping function $T(x)$ such that

$$X = \{T(x)|x \in X\}, T(T(x)) = x \tag{28}$$

and $f(T(x))J_T(x) + f(x) \approx 0$ where $J_T(x) = \|\mathrm{d}T(x)/\mathrm{d}x\|$. Assume that we sample primal sample x with pdf p. Then, we can calculate antithetic pdf p_T for antithetic sample $T(x)$ as follows:

$$p_T(T(x)) = \frac{p(x)}{J_T(x)}. \tag{29}$$

With primal and antithetic sample of x and $T(x)$ respectively, we get following antithetic estimator:

$$\langle I \rangle = 0.5\left(\frac{f(x)}{p(x)} + \frac{f(T(x))}{p_T(T(x))}\right). \tag{30}$$

Substituting p_T, we can rewrite the above as

$$\langle I \rangle = 0.5\left(\frac{f(x) + f(T(x))J_T(x)}{p(x)}\right). \tag{31}$$

It is important to note that $f(T(x))J_T(x)+f(x) \approx 0$, so the variance of $\langle I \rangle$ is also close to zero.

4.1 MIS between Primal and Antithetic Samples

We can consider MIS between primal and antithetic samples. In other words, primal sample x could be also sampled as an antithetic sample of another primal sample. Because $T(T(x)) = x$, the primal sample that makes x as an antithetic sample is $T(x)$. To utilize MIS between primal and antithetic samples, we have to calculate the following MIS weight,

$$w(x) = \frac{p(x)}{p(x) + p_T(x)} = \frac{p(x)}{p(x) + \frac{p(T(x))}{J_T(T(x))}} = \frac{p(x)}{p(x) + J_T(x)p(T(x))}, \tag{32}$$

$$w_T(T(x)) = \frac{p_T(T(x))}{p(T(x)) + p_T(T(x))} = \frac{\frac{p(x)}{J_T(x)}}{p(T(x)) + \frac{p(x)}{J_T(x)}} = \frac{p(x)}{p(x) + J_T(x)p(T(x))}. \tag{33}$$

Therefore, we can know that $w(p(x)) = w(p_T(T(x)))$. We only show a balance-heuristic, but it also works for arbitrary powers. Introducing MIS between primal and antithetic sampling replaces the constant 0.5 in Eq. (31) to MIS weight. Remember that the term $f(T(x))J_T(x) + f(x)$ remains the same, so we can still enjoy the advantage of using antithetic sampling.

4.2 MIS between Two Antithetic Strategies

Now let's consider MIS between two antithetic mapping function T_1, T_2. Note that primal sample that makes $T_1(x)$ as antithetic sample of T_2 is $T_2(T_1(x))$ (Fig. 10). Then, we need to calculate $p_{T_2}(T_1(x))$ and $p_{T_1}(T_2(x))$ to evaluate MIS weight between two strategies. This could be calculated as follows:

$$p_{T_2}(T_1(x)) = p_{T_2}(T_2(T_2(T_1(x)))) = \frac{p(T_2(T_1(x)))}{J_{T_2}(T_2(T_1(x)))}. \tag{34}$$

Using previously calculated pdf, we can evaluate MIS weight for

$$w_{T_1}(T_1(x)) = \frac{p_{T_1}(T_1(x))}{p_{T_1}(T_1(x)) + p_{T_2}(T_1(x))}. \tag{35}$$

We can do a similar process to calculate $w_{T_2}(T_2(x))$. For simplicity, let's represent $w_{T_1}(T_1(x)) = \alpha$ and $w_{T_2}(T_2(x)) = \beta$. Using these MIS

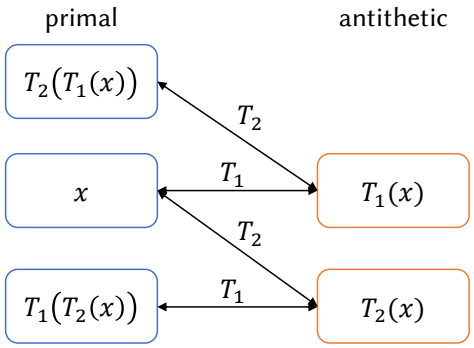

Fig. 10. Relationship between primal and antithetic samples.

weights, we can express antithetic estimator as

$$\begin{aligned}\langle I\rangle &= 0.5\frac{f(x)}{p(x)} + 0.5\left(\alpha\frac{f(T_1(x))}{p_{T_1}(T_1(x))} + \beta\frac{f(T_2(x))}{p_{T_2}(T_2(x))}\right)\\ &= 0.5\frac{f(x)}{p(x)} + 0.5\left(\alpha\frac{f(T_1(x))J_{T_1}(x)}{p(x)} + \beta\frac{f(T_2(x))J_{T_2}(x)}{p(x)}\right)\\ &= 0.5\frac{f(x) + \alpha f(T_1(x))J_{T_1}(x) + \beta f(T_2(x))J_{T_2}(x)}{p(x)}\end{aligned} \tag{36}$$

Note that we knows $f(T_1(x))J_{T_1}(x)+f(x) \approx 0$ and $f(T_2(x))J_{T_2}(x)+f(x) \approx 0$. However, unless $\alpha+\beta=1$, it is not guaranteed that the above Eq. (36) leverages the advantage of antithetic sampling. And in the general case, we cannot say that $\alpha+\beta=1$.

Here is one simple counter example when $x=(y,z)$:

$$\begin{aligned}f(y,z) &= \sin(y)\sin(z),\\ T_1(y,z) &= (y,-z),\\ T_2(y,z) &= (-y,z),\\ T_1(T_2(y,z)) &= T_2(T_1(y,z)) = (-y,-z).\end{aligned}$$

Note that $f(x)+f(T(x))J_T(x)$ is exactly zero and all of the Jacobian terms become 1. Then,

$$\begin{aligned}p_{T_2}(T_1(y,z)) &= \frac{p(T_2(T_1(y,z)))}{J_{T_2}(T_2(T_1(y,z)))} = p(-y,-z)\\ p_{T_1}(T_1(y,z)) &= \frac{p(y,z)}{J_{T_1}(y,z)} = p(y,z)\\ \alpha &= \frac{p(y,z)}{p(-y,-z)+p(y,z)}\end{aligned}$$

and

$$\begin{aligned}p_{T_1}(T_2(y,z)) &= \frac{p(T_1(T_2(y,z)))}{J_{T_1}(T_1(T_2(y,z)))} = p(-y,-z)\\ p_{T_2}(T_2(y,z)) &= \frac{p(y,z)}{J_{T_2}(y,z)} = p(y,z)\\ \beta &= \frac{p(y,z)}{p(-y,-z)+p(y,z)}.\end{aligned}$$

Unless $p(-y,-z)=p(y,z)$, $\alpha+\beta$ is not equal to one, which makes antithetic sampling not efficient for variance reduction.

REFERENCES

Mohit Gupta, Andreas Velten, Shree K. Nayar, and Eric Breitbach. 2018. What Are Optimal Coding Functions for Time-of-Flight Imaging? *ACM Transactions on Graphics* 37, 2 (April 2018), 1–18. https://doi.org/10/gd52p8

Yunpu Hu, Leo Miyashita, and Masatoshi Ishikawa. 2022. Differential Frequency Heterodyne Time-of-Flight Imaging for Instantaneous Depth and Velocity Estimation. *ACM Transactions on Graphics* 42, 1 (Sept. 2022), 9:1–9:13. https://doi.org/10/gspq2z

Ravi Ramamoorthi, John Anderson, Mark Meyer, and Derek Nowrouzezahrai. 2012. A Theory of Monte Carlo Visibility Sampling. *ACM Transactions on Graphics* 31, 5 (Sept. 2012). https://doi.org/10/gbbrnz

Received 20 February 2007; revised 12 March 2009; accepted 5 June 2009